RSC Advances

ROYAL SOCIETY OF CHEMISTRY

www.rsc.org/advances

Simultaneous adsorption of fluoride and hexavalent chromium by synthetic mesoporous alumina: performance and interaction mechanism

Tianguo Li[1], Daolei Xie[1], Changhua He[1], Xiaojun Xu[1] *, Bin Huang[2], Rui Nie[1], Shuli Liu[1], Zhengyang Duan[1], Wei Liu[1]

([1] Faculty of Environmental Science and Technology, Kunming University of Science and Technology, Kunming 650500, PR China;

[2] Institute of Environment and Life, Dalian University of Technology, Dalian 116023, PR China)

Abstract: The combined pollution of fluoride (F^-) and hexavalent chromium (Cr(VI)) in water bodies is getting much environmental concern of utmost priority. This study first evaluated the efficiency of simultaneous adsorption of F^- and Cr(VI) from aqueous solutions using a sol–gel–synthesized mesoporous alumina (MA) adsorbent. Adsorption properties showed that the sorption of F^- was spontaneity and endothermic, while Cr(VI) was nonspontaneous and exothermic in nature. Both the adsorption process was well described by the pseudo-second-order kinetics model and Langmuir isotherms. The maximum adsorption capacity is 14.39 and 9.19 mg/g for F^- and Cr(VI), respectively. F^- and Cr(VI) presents similar adsorption mechanism on MA adsorbent which primarily involved electrostatic attraction and chemisorption. The interaction adsorption experiments and FT-IR, XPS spectra demonstrated that the co-existence of F^- and Cr(VI) in solution impedes the sorption of Cr(VI) and accelerates the sorption of F^-. The former is ascribed to the competitive of surface adsorption active sites. The formation of surface chromium hydroxyl group ($\equiv CrOH$ or $\equiv CrOH_2^+$) could become a new adsorption sites for F^- adsorption which mainly contributes to the latter. Furthermore, these indicate that MA is a promising adsorption material for application to treatment of F^- and Cr(VI) combined pollution wastewater.

Key word: Fluoride; Hexavalent chromium; Mesoporous alumina; Simultaneous adsorption; Interaction mechanism

* Corresponding author. Tel.: +86 18787021530; fax: +86 0871 65920507. E-mail addresses: xuxiaojun88@sina.com (Xiaojun Xu).

1. Introduction

The combined pollution of fluoride and heavy metals is becoming a new topic and had been discovered in many industrial effluents.[1-7] Among them, chromium is a highly toxic heavy metal, which exists as negatively charged anion species, may be in the form of hydrogen chromate ($HCrO_4^-$), dichromate ($Cr_2O_7^{2-}$), chromate (CrO_4^{2-}) and H_2CrO_4 in solutions.[3-4] F^- and Cr(VI) co-pollution is a typical case of combined pollution and naturally occur in natural water and discharge from industrial processes such as mineral mining, processing and smelting, electroplating, dyeing, metal finishing, pigments, semiconductor and glass-manufacturing industries.[1-8] Both F^- and Cr(VI) in drinking water and dietary has significant advantage as well as toxic effects to human health depending on its acceptable daily intake. The permissible limits recommended by World Health Organization (WHO) for fluoride and total chromium in drinking water are 1.5mg/L and 0.05mg/L, respectively.[1, 3-4] However, the amount of both fluoride and Cr(VI) in natural water are in excess in many regions (India, Mexico, Africa, Pakistan and in some areas of China) of world due to anthropogenic pollution and natural release.[6] Fluoride in drinking water has a profound effect on teeth and bones. An appropriate content of fluoride (0.5–1.0mg/L) is required to prevent dental decay. However, excess ingestion of fluoride can induce dental fluorosis (1.5–4 mg/L), skeletal fluorosis (4–10 mg/L), even neurological damages.[6-10] Although trivalent chromium is an indispensable element to the body, Cr(VI) is highly biologic toxicity because of its mutagenicity, carcinogenicity and teratogenicity.[9-10] Therefore, it is of great importance to simultaneously control F^- and Cr(VI) from aqueous solutions.

The methods developed for removing excessive F^- or Cr(VI) from aqueous solutions respectively include precipitation,[11-12] electrocoagulation or electroflotation,[1, 13] membrane separation,[14-15] ion exchange,[16-17] electrodialysis,[18-19] adsorption,[2-3, 20-21] and others. Comparatively, adsorption is an available,

economical and environmental friendly technology for purifying wastewater contain F^- or Cr(VI). Different adsorbents (activated carbon, alumina, clay, chitosan beads and double layered hydroxides, etc.) have been investigated for the adsorption of F^- and Cr(VI).[5-9, 20, 25] Alumina is the most common sorbent and seems to be identified as the promising one.[5, 8, 22-24] For simultaneous removal of F^- and Cr(VI), a combined two-step electrocoagulation–electroflotation process had been used to remove F^- and Cr(VI) from acidic semiconductor effluents.[1] Nevertheless, limited adsorption works have been conducted to investigate the simultaneous removal of F^- and Cr(VI). For single sorption of F^- and Cr(VI), very promising results were obtained with alumina materials.[22-25] Although the adsorption of F^- and Cr(VI) separately by alumina had been studied, no study had explored in simultaneous removal of F^- and Cr(VI) by adsorption using a synthetic mesoporous alumina.

In the present study, a MA adsorbent was synthesized from inorganic aluminum sources and the simultaneous adsorption of F^- and Cr(VI) from aqueous solutions was investigated. Batch adsorption experiments were conducted to study various adsorption kinetic, isotherms and thermodynamic parameters. Attempts were also made to understand the interaction mechanism of F^-, Cr(VI) and MA adsorbent was analyzed with BET, TEM, FT-IR and XPS spectra. All results of this study would provide a reference as to the treatment of fluoride and Cr(VI) combined pollution wastewater.

2. Experimental section

2.1 Synthesis of MA adsorbent

Using the aluminium chloride ($AlCl_3 \cdot 6H_2O$) as inorganic aluminum source, MA was prepared by a procedure based on sol–gel and solvent evaporation-induced self-assembly (EISA) method with triblock copolymers P123 ($PEO_{20}PPO_{70}$ PEO_{20}) as template in an ethanol solutions.[26] In a typical synthesis,

approximately 1.0 g of P123 was dissolved in 20.0 mL of ethanol at room temperature and allowed to stir for 6 h. Then 2.04 g of $AlCl_3 \cdot 6H_2O$ and 1.6 mL of nitric acid (65–68 wt%) were added into the solution successively. The synthesis mixture was continuously stirred at room temperature for 12 h. Next, solvent was evaporated at 60°C for 48 h in air and a light-yellow solid was obtained. In order to get more perfect crystal phase and improve the ordering degree and thermostability of MA, re-crystallization was conducted by using a similar procedure reported by Luca.[27] Namely, the MA precursor was placed in 20.0 mL ethanol solutions and thermostatic back-flow for 12h at 80□. Then the mixture was transferred to a Büchner funnel, filtered by suction and dried in the oven at 60°C. The obtained samples were thermally treated in a muffle furnace by heating at 1°C/min to 400°C and then held at 400°C for 4 h to decompose the triblock copolymer template. Once cooled, MA were grounded and sieved to 200-300 meshes powder for later tests.

2.2 Batch adsorption experiments

The standard stock solutions of F^- and Cr(VI) were prepared by dissolving 2.21 g of sodium fluoride (NaF) and 2.83 g of potassium dichromate ($K_2Cr_2O_7$) into 1000 mL of deionized water, respectively. Batch adsorption experiments were conducted to determine the adsorption kinetic and equilibrium properties of F^- and Cr(VI) adsorbed on MA adsorbent. F^- and Cr(VI) simulation solutions with initial concentrations (C_0, mg/L) ranging from 2 to 100 mg/L selected were based on F^- and Cr(VI) contents generally present in actual effluents. The solution pH was adjusted to 6.0 with 0.10 mol/L NaOH or 0.10 mol/L HCl solutions. Adsorption experiments were performed by agitating 1.0 g/L of MA adsorbent with 200 mL of F^- and Cr(VI) solutions of desired concentrations at temperature from 25□ to 40□ in a 500 mL Teflon bottles. The bottle was capped tightly in a shaking machine operated at 120 rpm. At the end of predetermined time intervals, 20 ml of solution samples were taken, filtered with 0.45 um nylon sterile filters, and then the residual concentration (C_t, mg/L) of F^- and Cr(VI) was determined. Batch experiments were performed in

triplicate and the average values are reported. The adsorption amount (q_t, mg/g) at any time was calculated by the following equation:

$$q_t = \frac{V(C_0 - C_t)}{m} \quad (1)$$

Where, m (g) the weight of MA adsorbents, V (L) is the volume of solutions. For the modeling of the equilibrium data, three different kinetics models and two different isotherm equations were used to evaluate the kinetics, isotherms and mechanism of the adsorption process. The Equation of above models would be represented in corresponding chapters.

2.3 Analytical and characterization methods

The concentration of F^- was measured after mixing with total ionic strength adjustment buffer (TISAB III) by using a PF-1fluoride ion-selective electrode (Shanghai Ruosull Technology) with a PXSJ-216 Fion-meter (Shanghai Inesa Scientific).[28] The content of Cr(VI) in solution was determined by an atomic adsorption spectrometer (Agilent 240Z).

The nitrogen isotherms were determine by an ASAP 2000e analyzer (Quanta Co. Ltd.). Specific surface area of MA was obtained using the BET equation and the pore size distribution curve was calculated by the Barret–Joyner–Halenda (BJH) method using adsorption branch of the isotherms. The total pore volume was estimated from the adsorbed amount of nitrogen at a relative pressure P/P_0 of 0.99. Transmission electron microscopy (TEM) was conducted on a JEOL 2011 microscope (Japan) operated at 200 kV. Fourier transform infrared (FT-IR) spectra were obtained between 4000 and 400 cm^{-1} and recorded on a JASCO FT-IR 6100 spectrometer in transmittance mode in KBr. X-ray photoelectron spectroscopic (XPS) was measured on Shimadzu ESCA-750 spectrometers with Mg Kα X-ray sources.

3. Results and discussion

3.1 Characterization of MA

The nitrogen adsorption and desorption isotherms and their corresponding BJH pore size distributions of MA adsorbent is plotted in Fig.1 (a) and (b), respectively. The nitrogen sorption isotherms of MA show typical-IV curves with a H1-shaped hysteresis loop, suggesting the MA of mesoporous materials with cylindrical channels (Fig.1 (a)). TEM images (Fig.2) confirms that they possess mesostructure. After re-crystallization and thermal treatment at 400°C, MA synthesized exhibits a larger specific surface area is 211.4 m^2/g and its total pore volume is 0.54 cm^3/g. From BJH pore size distribution (Fig.1 (b)), it can be learned that MA displays a narrow distribution and mainly centre at 6–11nm, indicating that MA has a uniform pore size with average pore diameter at 8.4nm.

3.2 Adsorption kinetics studies

Contact time controls the adsorption process at the water/adsorbent interfaces. Hence, adsorption equilibrium time was done by studying the uptake of F^- and Cr(VI) over MA adsorbent. Fig.3 (a) shows the adsorption efficiency of F^- and Cr(VI) by MA as a function of time at pH 6, and the initial concentration of F^- and Cr(VI) was 50 mg/L and 100 mg/L, respectively. The adsorption efficiency of both F^- and Cr(VI) increases as the contact time increased. There were negligible change in the residual concentration of both F^- and Cr(VI) and reached an equilibrium value beyond 12h.

Three typical kinetic models, pseudo-first-order, pseudo-second-order and intraparticle diffusion model were applied to examine the adsorption kinetics of F^- and Cr(VI) on MA adsorbent (Fig.3 (b, c, d). The kinetic parameters estimated by the three models are presented in Table 1. It is evident that pseudo-second-order model better fits the experimental data than other models, with correlation values (R^2) quite close to unity and theoretical values of calculated equilibrium adsorption capacities (q_e)， which is

closer to the experimental equilibrium values. These indicate that chemisorption is a prevailing mechanism for F^- and Cr(VI) adsorbed on MA adsorbent. The sorption process involves transport of F^- and Cr(VI) ions by diffusion process and adsorption equilibrium.[23-24] The correlation value favors the intraparticle diffusion process as the rate-limiting step. The plateaus are more notorious and the linear portion of all plots (Fig.3 (d)) is not passing through the origin indicated that the sorption of F^- and Cr(VI) on MA adsorbent is a complex process.[14] The slope and intercepts of the plots increased with increasing the initial concentrations may be attributed to the growing effect of concentration gradient and external mass transfer resistance. The adsorption of F^- and Cr(VI) in composite system co-existence of both elements shows similar kinetics feature with single system. The adsorption rate constants (k) and capacity (q_e) of F^- improved when co-existence with Cr(VI), while Cr(VI) shows the opposite effect. From the characteristics of adsorption kinetics and mesoporous property of MA, it might be concluded that both surface adsorption and intraparticle diffusion contribute to the rate-limiting step for F^- and Cr(VI) adsorbed on MA adsorbent which are consistent with the literature reported.[23-25]

3.3 Adsorption isotherm studies

Adsorption isotherms not only help in determining the effectiveness of the MA adsorbents in removing F^- and Cr(VI) from aqueous solution, but also provide a general idea of the maximum adsorption capacity (q_m). Langmuir and Freundlich isotherms were employed to provide a deep insight into the mode of adsorption of F^- and Cr(VI) on MA adsorbent. The adsorption isotherms of F^- and Cr(VI) in single and composite system on MA adsorbents are shown in Fig.4 and the equilibrium constants are given in Table 2. The isotherms in single and composite system are positive, regular and concave to the concentration axis. The high values of regression coefficients (R^2) show that both Langmuir (≥ 0.973) and Freundlich (≥ 0.975) equation provide an accurate description of the experimental data. These indicated that both monolayer

adsorption and heterogeneous surface conditions exist under the adsorption situations.[27] The Langmuir model gave a better fitting to the experimental data than Freundlich for F^- adsorption, while reverse for Cr(VI) adsorption, relatively. The adsorption intensity of 1/n lies between 0.1 and 1, were less than unity, indicating a favourable adsorption and formation of relatively stronger bond between adsorbate (F^- and Cr(VI)) and MA adsorbent.[22-23] The monolayer surface coverage, q_m of F^- increased and q_m of Cr(VI) decreased with increase of T on the reaction, respectively. The q_m of F^- obtained was 14.39 mg/g at temperature of 40□, while Cr(VI) was 9.19 mg/g at temperature of 25□. In composite system of F^- and Cr(VI), both of the Langmuir equilibrium adsorption constant (b) and Freundlich empirical constants (K) larger than which in single system. The adsorption isotherms of F^- and Cr(VI) on MA adsorbent is more steep than single system but q_m obtained was decreased. These phenomena indicate that the presence of Cr(VI) (50mg/L) in the promotion of F^- adsorption on MA adsorbent in low F^- concentration solution, while it shows competition mechanism in high F^- concentration solution. Similarly as the adsorption of Cr(VI) when co-existence with F^- (50mg/L) and the q_m of Cr(VI) decreased more dramatically than F^-. The variation of isotherms characteristics suggested that the F^- and Cr(VI) may share same adsorption sites on MA surface and there exists the competitive adsorption phenomena. Hence, it could be concluded that Langmuir isotherm should be a more descriptive model for simultaneous adsorption of F^- and Cr(VI).

3.4 Thermodynamic parameters evaluation

Thermodynamic analysis is very important to illustrate the sorption mechannism and conclude whether the process is spontaneous or nonspontaneous. Thermodynamic parameters are calculated from the variation of the adsorption equilibrium constant K_c with changes in temperature. The equilibrium constant K_c is expressed as Eq. (2).[29]

$$K_c = \frac{\alpha_s}{\alpha_e} = \frac{\nu_s C_s}{\nu_e C_e} \quad (2)$$

Where α_s is the activity of the adsorbed solute, α_e the activity of the solute in the equilibrium solution, C_s is the surface concentration of F^- and Cr(VI) in mg/g of exchanger, namely equilibrium adsorption capacity and C_e the concentration of F^- and Cr(VI) in equilibrium solution in mg/L, ν_s and ν_e the activity coefficient of the adsorbed solute and the solute in the solution.

For dilute solution and monolayer adsorption, the activity coefficient approaches unity. Eq. (2) can be written as Eq. (3).

$$\frac{C_s}{C_e} = \frac{\alpha_s}{\alpha_e} = K_c \quad (3)$$

Values of K_c are obtained by calculated from adsorption equilibrium date at lower concentration. Then, ΔG°, ΔH°, and ΔS° were evaluated using the following standard Eq. (4) and Eq. (5).[23, 29]

$$\Delta G^0 = -RT \ln K_c \quad (4)$$

$$\ln K_c = \frac{\Delta S^0}{R} - \frac{\Delta H^0}{RT} \quad (5)$$

Where R is the universal gas constant (8.314 J/(mol.K)). The values of ΔH° and ΔS° can be calculated from the slope and intercept of a plot of $\ln K_c$ versus 1/T, respectively. Fig.5 demonstrates the plot of $\ln K_c$ versus 1/T in accordance to Eq. (5) and the values of thermodynamic parameters are presented in Table 3. In the case of F^- adsorption, the negative values of ΔG^0 indicated that the spontaneity of the adsorption process under the condition reaction. The ΔG^0 values increased gradually with increasing T value (Table 3) indicated that the spontaneous nature of F^- adsorption reaction increased with rising T value. The standard enthalpy change (ΔH^0) was positive show that the F^- adsorption process was of an endothermic in nature. While the adsorption process was of an exothermic and nonspontaneous in nature for Cr(VI).[32] From the magnitude of ΔH^0 means that the dominated attachment of both F^- and Cr(VI) with MA takes place via electrostatic attraction forces.[20] The positive value for the entropy change (ΔS°) of fluoride reflected that the adsorption reaction took place with increasing entropy. While the negative values of the entropy change

(ΔS°) indicate a favorable adsorption process of Cr(VI). This may due to the increase of randomness with increase in number of species at the solid–liquid interface of F^- and Cr(VI). But the formation of adsorbed Cr(VI) has a stable structure, which is beneficial to decrease the randomness of Cr(VI) species relatively although the randomness of always goes up in the system.

3.5 Interaction mechanisms

3.5.1 Interaction effects and mechanisms

In order to understand the interactional effects and mechanisms, the adsorption of F^- (Cr(VI)) as a function of co-existence with different concentration of Cr(VI) (F^-) were investigated.Fig.6 (a) shows the removal efficiency of F^- increased with the increase of Cr(VI) in solution, which reveals that co-existence of Cr(VI) in solution accelerates the sorption of F^-. Whereas adding F^- in solution is obstacles for the sorption of Cr(VI). Several reasons may be contribute to these interaction phenomena. It is known that Cr(VI) exists as negatively charged anion species ($HCrO^{4-}$, $Cr_2O_7^{2-}$ CrO_4^{2-} and H_2CrO_4) in solution depending on solution environment and displays anion-type sorption behavior similar with F^-.[3-4, 24] The co-existence of fluoride and Cr(VI) species in wastewater may compete for the adsorption sites on surface of MA adsorbent. As the foregoing analysis, both F^- and Cr(VI) can uptake onto MA surface might via electrostatic attraction or chemisorption, namely formation of chemical bond between MA with adsorbate and the available reaction types are described in Fig.7. Aluminum oxides located in solution have surface hydroxyl sites ($\equiv AlOH$) and can generate $\equiv AlOH_2^+$, $\equiv AlO^-$ and $\equiv Al^+$ through deprotonation-protonation and hydration (Eq. (6-7)).

$$\equiv AlOH + H^+ \rightarrow \equiv AlOH_2^+ \rightarrow \equiv Al^+ + H_2O \quad (6)$$

$$\equiv AlOH \rightarrow \equiv AlO^- - H^+ \quad (7)$$

The electrostatically attract interaction of F^- and Cr(VI) species between the MA surface $\equiv AlOH_2^+$

forms on outer sphere complexes $\equiv AlOH_2^+ \cdots X$ (Fig.7 (a), (e) and (g)), where X on behalf of the F^- and Cr(VI) species.[30] These outer sphere complexes can further form much stabler inner sphere complexes $\equiv Al \cdots X$ via dehydration (Fig.7 (d), (f) and (h-j)).[31-32] Furthermore, the interaction adsorption mechanism also contain the substitution of hydroxyl group with F^- to form $\equiv AlF$ (Fig.7 (d)), or fluoride and Cr(VI) species directly coordination with MA surface hydroxyl (Fig.7 (c)). Consequently, it attributed fluoride co-exists in solution weighted against the adsorption of Cr(VI) to the competitive effect of internal diffusion of contamination and surface adsorption active sites. As shown in Fig.7 (k-m), the promotional effect of F^- sorption in presence of Cr(VI) in solution may due to the Cr(VI) species adsorbed on MA surface forming a new surface hydroxyl group ($\equiv CrOH$ or $\equiv CrOH_2^+$) which being a new adsorption sites for F^-. However, the removal capability of F^- and Cr(VI) exhibits no noticeable effect when they are in co-existence with appropriate range of content, indicating that the MA adsorbents can achieve the simultaneous removal of F^- and Cr(VI) from aqueous solution.

3.5.2 FT-IR spectra characterization

The above results suggested that the adsorption of F^- and Cr(VI) ions onto MA adsorbent may be a complex process involving both physical and chemical sorption. To get a better insight to the nature of the interactions mechanism of F^-, Cr(VI) and MA adsorbent solution system, the FT-IR spectra of MA before and after adsorption (single or simultaneous) were analyzed and present in Fig.8. The MA powder as such has shown characteristic absorption bands at 599.8, 867.9, 1116.7, 1425.3, 1525.6, 1643.3, 2925.9, and 3456.3 cm^{-1}. As for these spectra before and after absorption of F^- and Cr(VI), the absorption bands at 2925.9-3456.3 cm^{-1} and 1637.5 cm^{-1} are respectively ascribed to the stretching and bending vibration of the hydroxyl groups and there are showing no obviously variation except the intensity.[31-33] When F^- was adsorbed, the disappearance of sharp band peak of 1116.7 cm^{-1} assigned to the bending vibration of Al–OH

most likely be attributed to substitution of hydroxyl groups by F^-.[35-36] Additionally, the broad peak of Al–O bond shifting from 599.8 cm^{-1} to 576.7 cm^{-1} is due to the effect of Al-F stretching vibrations.[32, 36] It is worth noting that the appearance of a sharp band at 2345.4 cm^{-1} and 2027.1 cm^{-1} after F^- was adsorbed may be indicative of formation of a new chemical bond on the MA surface which needed further verifying. When Cr(VI) was adsorbed, the appearance of new peak at 869.9 cm^{-1} is corresponded to stretching and bending modes of Cr-O of chromate (CrO_4^{2-}) which indicates the occurrence of Cr(VI) adsorption on MA adsorbent.[1, 9] In the case of simultaneous adsorption of F^- and Cr(VI), the new peak of band at 418.5 cm^{-1} indicating that there are some interaction between F^- and Cr(VI) species at the interface of MA adsorbent soild-liquid, except characteristics of FT-IR spectra of MA adsorbent after single adsorbed F^- and Cr(VI), respectively.[31-32, 35]

3.5.3 XPS spectra characterization

The XPS spectra were used to determine the chemical states and coordination of F^- and Cr(VI) adsorbed onto the MA adsorbents. Fig.9 shows their F 1s, Cr 2p, Al 2p and O 1s XPS spectra of the MA adsorbents after different adsorption situations. For single F-loaded adsorbent, F peak was observed near 686 eV and the F 1s spectrum was divided into four peaks at 684.7, 686.2, 687.9 and 690.5 eV which can be assigned to alkali metal fluoride (Na(K)-F), aluminum fluoride (Al–F), aluminum hydroxide fluoride (Al-FOH) and fluorocarbon (C-F) due to carbon impurity (Fig.9 (a)), respectively.[40-42] The observed alkali metal fluoride indicated that F^- might be adsorbed in following mechanism (Eq. (8)).

$$MA.\alpha H_2O_{(s)} + Na^+ + F^- \rightarrow MA(\alpha - 1)H_2O.OH^-Na^+F + H^+ \quad (8)$$

When F^- and Cr(VI) were adsorbed simultaneously, the F 1s peak shifted towards the lower binding energy and the peaks intensity of 685.9 eV, 687.2 eV increased in comparison to the single F^- adsorption. These indicating fluoride and Cr(VI) species were effectively adsorbed onto the adsorbent surface and

interacting with each other which was in accordance with the results of FT-IR spectra. From the high-resolution scan of Cr 2p3/2, there are presence of Cr(III) and Cr(VI) on the adsorbent surface at 576.0–577.8 eV and 579.4–579.8 eV, respectively ((Fig.9 (c) (d))), indicating that the hexavalent chromium was reduced to trivalent chromium during the sorption process.[3, 9, 34, 38-39] Compared with Cr(VI)-loaded adsorbent (Fig.9 (c)) and F, Cr(VI) co-loaded adsorbent (Fig.9 (d)), it can be seen that Cr 2p3/2 spectra has no significantly difference in peak position and intensity.

Fig.9 (e-g) and (h-j) illustrates the Al 2p and O1s spectra of the pristine MA, F-loaded MA and F, Cr(VI) co-loaded MA adsorbent, respectively. The dominant Al 2p peak is occurred at 74.1 eV and 75.2 eV for pristine MA adsorbent, which can be assigned to aluminum oxide (Al-O) and aluminum hydroxides (Al-OH) respectively.[40-41] The new peak was observed at 76.3 eV demonstrating the formation of aluminum fluoride (Al-F) on MA surface after single F^- sorption. Similarly, it can be seen that the O 1s spectra can be deconvoluted into three components at near 530.7, 531.9 and 533.4 eV, which can be assigned to metal oxide (M-O), metal hydroxides or hydroxyl groups (-OH) and adsorbed water (H_2O).[34, 39, 41] Both the peaks intensity Al 2p of Al-OH and O 1s of -OH decreased after F^- adsorption, suggesting that one of the adsorption mechanisms of F^- is the replacement for hydroxyl groups with F^-.[3, 40] By comparison of single and simultaneous adsorption, the atomic ratio for the O 1s peak at 530.5 eV attributed to M-O increased from 29.55% to 39.44% showing that the adsorption of Cr(VI) takes place on MA surface. But it was amazing that the atomic ratio of O 1s of metal hydroxides (-OH) decreased from 56.09% to 49.23%, while the atomic ratio for the Al 2p peak at 74.8 eV which belongs to Al-OH increased from 7.65% to 33.81%. This strong contrast phenomenon proved clearly that the took place of chemical reactions between F^- and Cr(VI) species on MA surface which was consistent with the interaction mechanism proposed above (Fig.7).`In this way, the sorption of Cr(VI) species on MA surfaces in the form of monolayer coverage and

the relative distribution of –OH in dichromate ions is lower the surface aluminum (≡AlOH). So that the simultaneous adsorption of Cr(VI) changed the atomic ratio of O 1s and made the chemical species of metal hydroxides (-OH) decrease. Although the content of Al was reduced, the substitution of hydroxyl groups by fluoride partial reaction with the $\equiv CrOH$ bonds and the strengthened protonation of ≡AlOH and ≡AlO (Eq. 6) might contribution to the relative distribution of AlOH bonds increased significantly.

4. Conclusions

This present study describes the first attempt of simultaneous adsorption of F^- and Cr(VI) from combined pollution wastewater by an inorganic alumina sol–gel-derived MA adsorbent. Experimental data shows better agreement with the pseudo-second-order model, and the rate-limiting step for both F^- and Cr(VI) adsorbed on MA adsorbent controlled by surface adsorption and intraparticle diffusion process. The adsorption process can be well described by the Langmuir isotherm for F^- adsorption, while better fit with the Freundlich isotherm for Cr(VI) adsorption, relatively. Thermodynamic parameters such as ΔH^0, ΔS^0 and ΔG^0 obtained exhibit that the adsorption process of F^- was spontaneity and endothermice, while Cr(VI) of was nonspontaneous and exothermic in nature. Even though the co-existence of F^- and Cr(VI) is obstacles for the sorption of Cr(VI), the re-crystallization product of MA powder can be an effective adsorbent for simultaneous adsorption of F^- and Cr(VI) from wastewater. The maximum adsorption capacity is 14.39 mg/g at 40℃ and 9.19 mg/g at 25℃ for F^- and Cr(VI), respectively. The adsorption performance and FT-IR, XPS spectra indicated that the adsorption mechanism for F^- and Cr(VI) on MA involved electrostatic attraction and chemisorption occurs primarily through the formation of $\equiv AlOH_2^+ \cdots X$, $\equiv Al \cdots X$ complexes. It demonstrated clearly that the MA adsorbed Cr(VI) species ($\equiv CrOH$, $\equiv CrOH_2^+$) forming a new sorption sites for the adsorption of F^- was the primary interaction mechanism.

Acknowledgement

The financial support of this work was provided by the Scientific Research Fund of Yunnan Provincial Department of Education（2013Y327）and Analysis and Measurement Funds of Kunming University of Science and Technology (20140550, 20150460).

References

[1] S. Aoudj, A. Khelifa, N. Drouiche, R. Belkada and D. Miroud, Chem. Eng. J., 2015, **267**, 153–162.

[2] R. Rakhunde, L. Deshpande, H. D. Juneja, Environ. Sci. Technol., 2012, **42**, 776–810.

[3] Y. Wang, D. F. Liu, J. B. Lu, J. Huang, Colloids Surf. A: Physicochem. Eng. Aspects, 2015, **481**, 133–142.

[4] Q. Cheng, C. W. Wang, K. Doudrick, C. K. Chan and Appl. Catal. B - Environ., 2015, **176–177**, 740–748.

[5] S. X. Teng, S. G. Wang, W. X. Gong, X. W. Liu and B. Y. Gao, J. Hazard. Mater., 2009, **168**, 1004–1011.

[6] T. Rafique, S. Naseem, M.I. Bhanger and T.H. Usmani, Environ. Geol., 2008, **56**, 317–326.

[7] A. Tor, N. Danaoglu, G. Arslan and Y. Cengeloglu, J. Hazard. Mater., 2009, **164**, 271–278.

[8] M. Mohapatra, S. Anand, B.K. Mishra, Dion E. Giles and P. Singh, J. Environ. Manage., 2009, **91**, 67–77.

[9] L. Li, Y. X. Li, L. X. Cao and C. F. Yang, Carbohyd. Polym., 2015, **125**, 206–213.

[10] M. Narayani and K. V. Shetty, Crit. Rev. Environ. Sci. Technol., 2013, **43**, 955–1009.

[11] P. Miretzky and A.F. Cirelli, J. Fluorine Chem., 2011, **132**, 231–240.

[12] A. K. Golder, A. K. Chanda, A. N. Samanta and S. Ray., Sep. Purif. Technol., 2011, **76**, 345–350.

[13] K. Singh, D. H. Lataye, K. L. Wasewar and C. K. Yoo, Desalin. Water Treat., 2013, **51**, 3233–3247.

[14] J. J. Shen, G. Mkongo, G. Abbt-Braun, S. L. Ceppi, B. S. Richards and A. I. Schäfer, Sep. Purif. Technol., 2015, **149**, 349-361.

[15] G. R. Xu, J. N. Wang and C. J. Li, Chem. Eng. J., 2012, **198–199**, 310-317.

[16] L. N. Ho, T. Ishihara, S. Ueshima, H. Nishiguchi and Y. Takita, J. Colloid Interf. Sci., 2004, 272, 399-403.

[17] L. Alvarado, I. R. Torres and A. C. Chen, Sep. Purif. Technol., 2013, **105**, 55–62.

[18] N. Kabay, Ö. Arar, S. Samatya, Ü. Yüksel and M. Yüksel, J. Hazard. Mater., 2008, **153**, 107-113.

[19] O. Scialdone, A. D'Angelo, E. D. Lume and A. Galia, Electrochimica Acta, 2014, **137**, 258–265.

[20] K. Biswas, K. Gupta, A. Goswami and U. C. Ghosh, Desalination, 2010, **255**, 44–51.

[21] X. T. Sun, L. R. Yang, H. F. Xing, J. M. Zhao, X. P. Li and Y. B. Huang, Chem. Eng. J., 2013, **234**, 338–345.

[22] E. Kumar, A. Bhatnagar, U. Kumar and M. Sillanpää, J. Hazard. Mater., 2011, **186**, 1042–1049.

[23] R. P. Liu, W. X. Gong, H. C. Lan, Y. P. Gao, H. J. Liu and J. H. Qu, Chem. Eng. J., 2011, **175**,144–149.

[24] T. J. Reich and C. M. Koretsky, Geochim. Cosmochim. Ac., 2011, **75**, 7006–7017.

[25] E. Alvarez-Ayuso, A. Garcia-Sanchez and X. Querol, J. Hazard. Mater., 2007, **142**, 191–198.

[26] Q. Yuan, A. X. Yin and C. Luo, J. Am. Chem. Soc., 2008, **130**, 3466-3467.

[27] V. Luca and J. M. Hook, Chem. mater., 1997, **9**, 2731-2744.

[28] F. S. Wei, China Environmental Science Press, Beijing, 2002, 189–193.

[29] A. A. Khan' and R. P. Singh, Colloids and Surfaces, 1987, **24**, 33-42.

[30] P. Somasundaran, Taylor and Francis, 2006.

[31] M. Kumari, C. U. Pittman Jr. and D. Mohan, J. Colloid Interf. Sci., 2015, **442**, 120–132.

[32] S. S. Thakur and G. S. Chauhan, Ind. Eng. Che. Res., 2014, **53**, 4838−4849.

[33] M. Karthikeyan and K. P. Elango, J. Environ. Sci-China, 2009, **21**, 1513–1518.

[34] S. B. Deng, H. Liu, W. Zhou, J. Huang and G. Yu, J.Hazard. Mater., 2011, **186**, 1360–1366.

[35] M. G. Sujana and S. Anand, Applied Surface Science, 2010, **256**, 6956–6962.

[36] U. Gross, S. Rüdiger, E. Kemnitz, K. Brzezinka, S. Mukhopadhyay, C. Bailey, A. Wander and N. Harrison, J. Phys. Chem. A, 2007, **111**, 5813–5819.

[37] L. Chen, H. X. Wu, T. J. Wang, Y. Jin, Y. Zhang and X. M. Dou, Powder Technol., 2009, **193**, 59–64.

[38] F. Cavani, M. Koutyrev, F. Trifiro, A. Bartolini, D. Ghisletti, R. Iezzi, A. Santucci and G. D. Piero, J. Catalysis, 1996, **58**, 236–250.

[39] D. J. Kang, X. L. Yu, S. R. Tong, M. F. Ge, J. C. Zuo, C. Y. Cao and W. G. Song, Chem. Eng. J., 2013, **228**, 731–740.

[40] T. Skapin, Z. Mazej, A. Makarowicz, A. Jesih, M. Nickkho-Amiry and S. L. M. Schroeder, J. Fluorine Chem., 2011, 132, 703–712.

[41] N. Reddy, P. Bera, V. R. Reddy, N. Sridhara, A. Dey, C. Anandan and A. K. Sharma, Ceram. Int., 2014, **40**, 11099–11107.

[42] W. Kleist, C. Haebner, O. Storcheva and C. Kohler, Inorg. Chem. Acta, 2006, **359**, 4851–4854.

Table 1 Kinetics parameters for F^- and Cr(VI) adsorption on MA adsorbent at different initial concentrations and systems

Item	Initial con. (mg/L)	Pseudo-first-order $q_t = q_e(1 - e^{-k_1 t})$			Pseudo-second-order $q_t = q_e^2 k_2 t/(1 + q_e k_2 t)$			Intraparticle diffusion $q_t = k_i t^{1/2} + 1$	
		k_1 (min^{-1})×10^{-2}	q_e (mg/g)	R^2	k_2 (g.mg^{-1} min^{-1})×10^{-3}	q_e (mg/g)	R^2	k_i (g (mg^{-1} $min^{0.5}$)	R^2
Adsorption of F^-	30	0.92	4.83	0.948	2.19	5.40	0.986	0.16	0.928
	50	0.94	6.92	0.955	1.57	7.72	0.985	0.25	0.948
	50 [a]	1.85	7.92	0.965	3.06	8.55	0.984	0.34	0.704
Adsorption of Cr(VI)	50	1.01	4.03	0.921	3.05	4.46	0.973	0.12	0.913
	100	1.89	6.83	0.912	3.54	7.40	0.980	0.28	0.786
	100 [b]	0.97	5.85	0.943	1.97	6.49	0.977	0.21	0.941

'a' the adsorption of F^- in solution F^- (50mg/L) co-existence with 50mg/L Cr(VI), 'b' the adsorption of Cr(VI), in solution Cr(VI) (100mg/L) co-existence with 50mg/L F^-.

Table 2 Langmuir and Freundlich isotherm constants for F^- and Cr(VI) adsorption on MA adsorbents

Contaminant		Temp. (℃)	Langmuir isotherm $q_e = Q_{max} * b * C_e/(1 + b * C_e)$			Freundlich isotherm $q_e = K * C_e^{1/n}$		
			Q_{max} (mg/g)	b (L/mg)	R^2	K	1/n	R^2
Adsorption of F^-	Single F^-	25	12.00	0.121	0.999	1.65	0.56	0.987
		30	12.73	0.130	0.999	1.82	0.56	0.988
		35	13.37	0.131	0.999	1.88	0.58	0.987
		40	14.39	0.135	0.999	1.94	0.59	0.988
	F^- co-exist with 50mg/L Cr(VI)	25	11.68	0.166	0.987	2.318	0.486	0.981
		30	12.24	0.215	0.991	2.484	0.518	0.980
		35	12.27	0.261	0.981	2.825	0.495	0.975
		40	12.49	0.319	0.978	3.244	0.481	0.980
Adsorption of Cr(VI)	Single Cr(VI)	25	9.19	0.039	0.986	0.84	0.50	0.999
		30	8.85	0.038	0.988	0.76	0.52	0.999
		35	8.61	0.036	0.987	0.70	0.52	0.983
		40	8.27	0.035	0.987	0.64	0.53	0.997
	Cr(VI) co-exist with 50mg/L F^-	25	8.10	0.101	0.991	1.56	0.38	0.986
		30	8.02	0.085	0.975	1.45	0.38	0.985
		35	7.47	0.105	0.982	1.59	0.35	0.986
		40	6.48	0.182	0.973	1.87	0.29	0.990

Table 3 Thermodynamic parameter for F^- and Cr(VI) adsorption at different temperatures

Contaminant	Temp. (□)	ΔG° (kJ/mol)	ΔH° (kJ/mol)	ΔS° (kJ/mol/K)
F	25	-0.683	13.79	0.048
	30	-1.065		
	35	-1.260		
	40	-1.426		
Cr(VI)	25	1.181	-32.96	-0.115
	30	1.946		
	35	2.386		
	40	3.788		

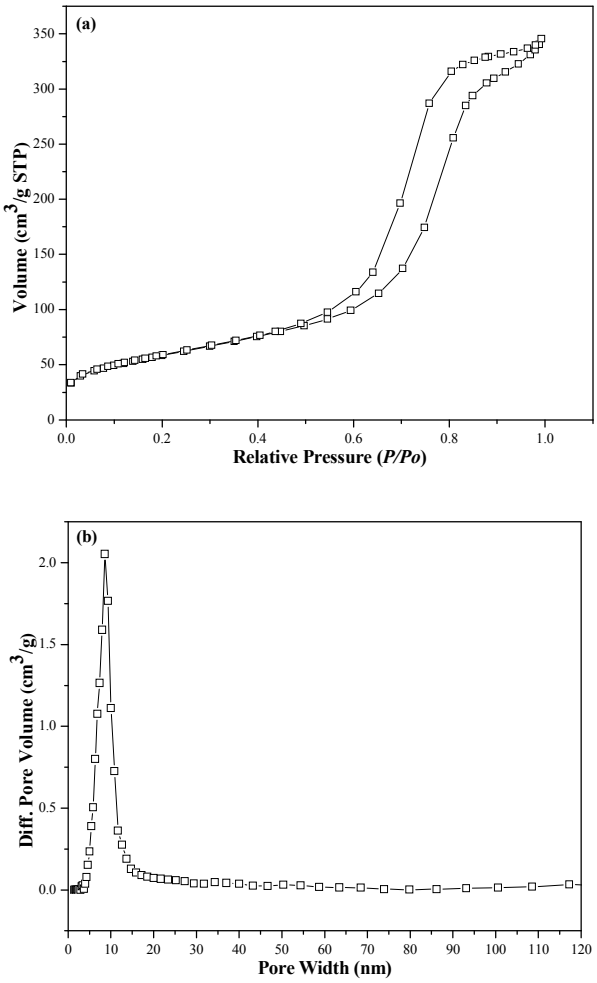

Fig.1 (a) Nitrogen adsorption/desorption isotherms and (b) BJH pore size distributions on MA adsorbents

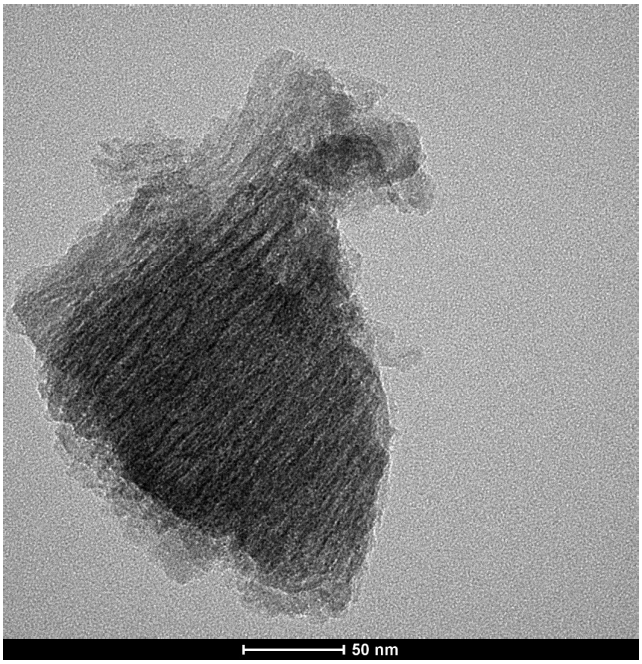

Fig.2 TEM images of the MA adsorbents

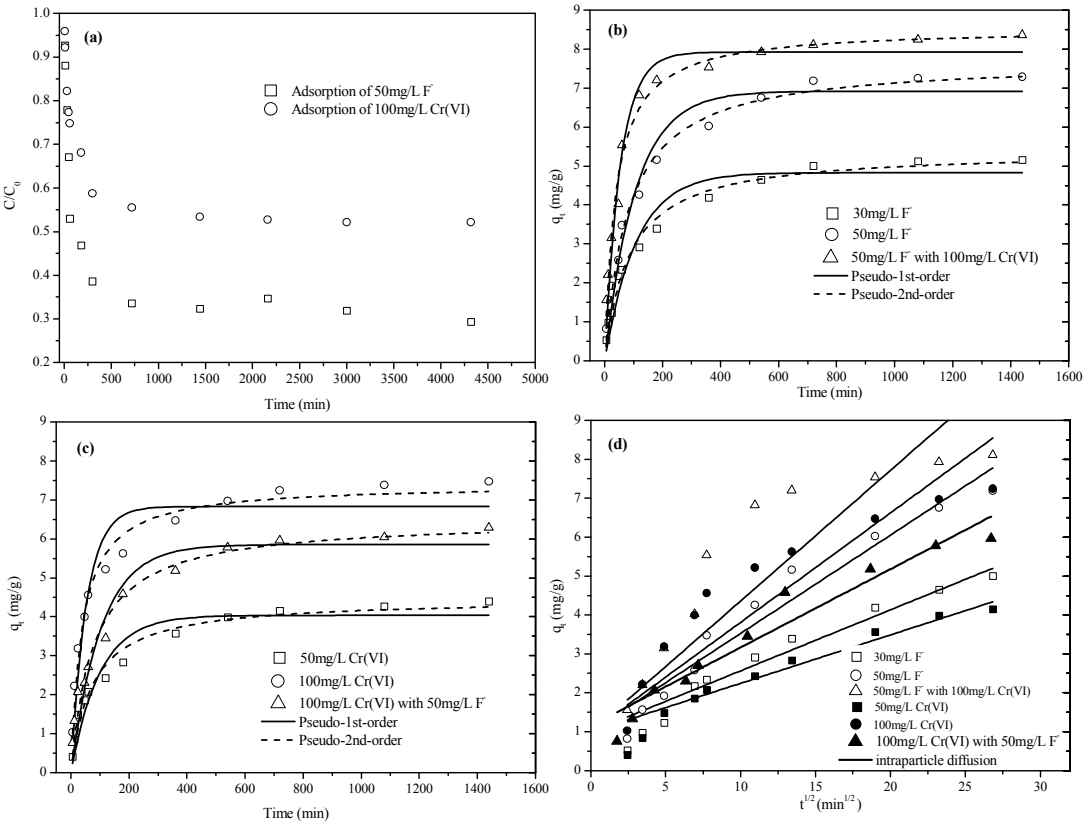

Fig.3 (a) The plot of C/C_0 versus t (min) for the F^- and Cr(VI) adsorption on MA adsorbent, (b) Pseudo-first-order, Pseudo-second-order plots for F^- adsorption on MA adsorbent, (c) Pseudo-first-order, Pseudo-second-order sorption kinetics for Cr(VI) adsorption on MA adsorbent, (d) Intraparticle diffusion model for F^- and Cr(VI) adsorption on MA adsorbent (Experiment conditions: pH = 6 ± 0.2, adsorbent dosage = 1 g/L, T = 25 ± 2℃)

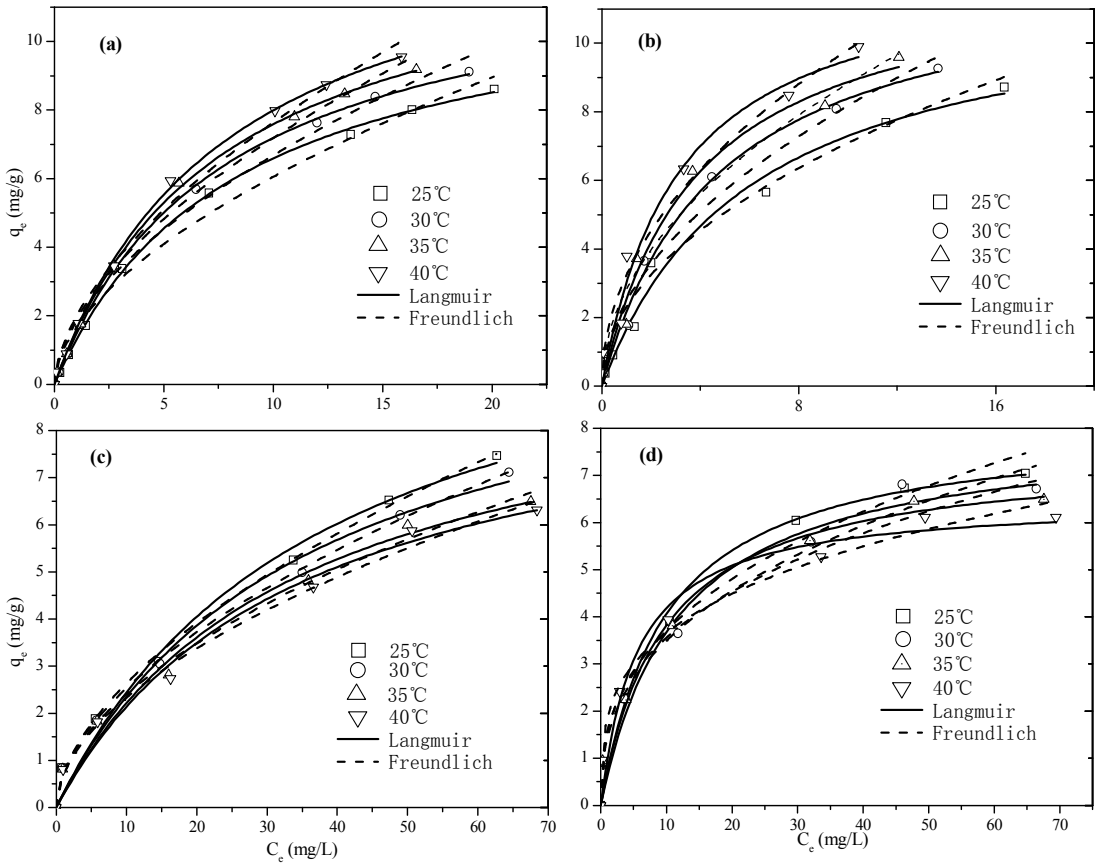

Fig.4 Adsorption isotherms of F^- and Cr(VI) on MA adsorbent modeling using the Langmuir and Freundlich equations (a) single F^-, (b) F^- co-existence with 50mg/L Cr(VI), (c) single Cr(VI), (b) Cr(VI) co-existence with 50mg/L F^- (Experiment conditions: pH = 6 ± 0.2, adsorbent dosage = 1 g/L, T range from 25℃ to 40℃)

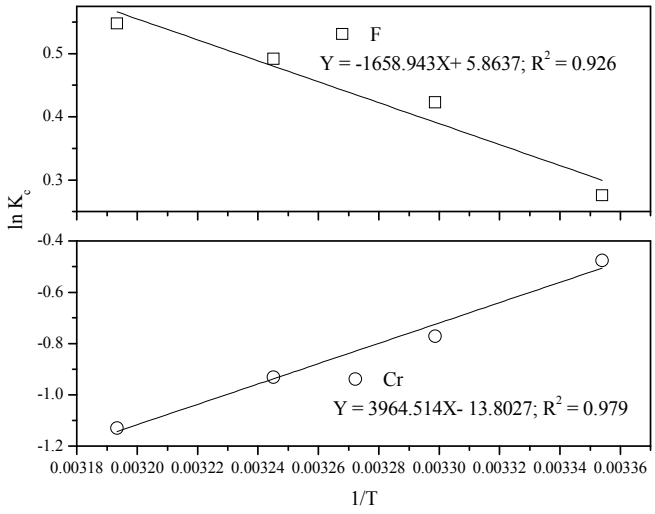

Fig.5 Thermodynamic plot of ln K_c as a function of the reciprocal of temperature (1/T) for the adsorption of F^- and Cr(VI) by MA adsorbent

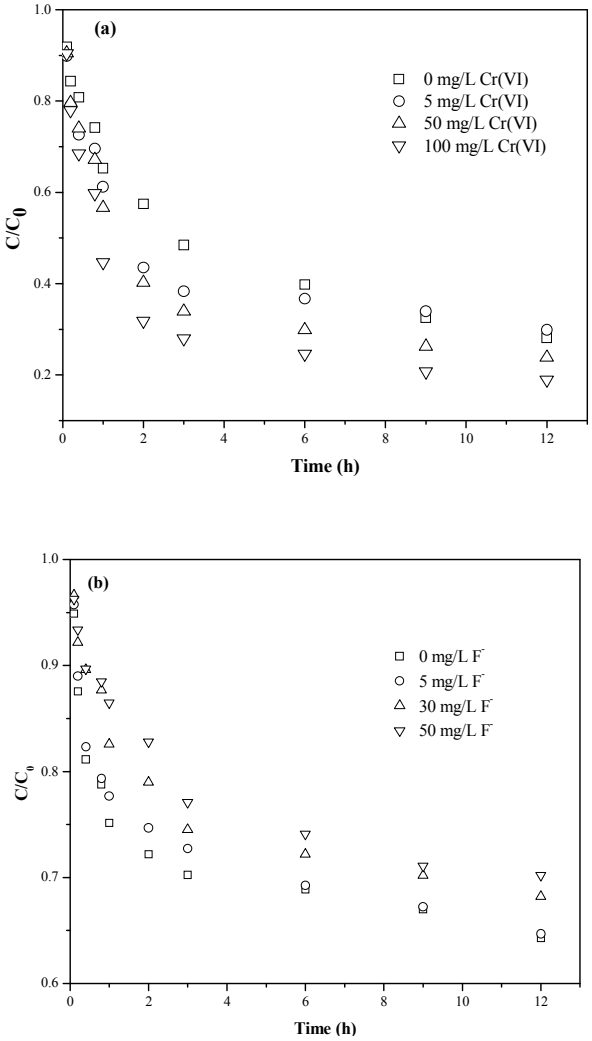

Fig.6 (a) Effect of different Cr(VI) concentration on F^- sorption onto MA powder, (b) effect of different F^- concentration on Cr(VI) sorption onto MA powder (Experimental conditions: pH = 6 ± 0.2, adsorbent dosage = 1 g/L, T =25 ± 2℃, initial concentration of F^- and Cr(VI) was 50mg/L and 100mg/L, respectively)

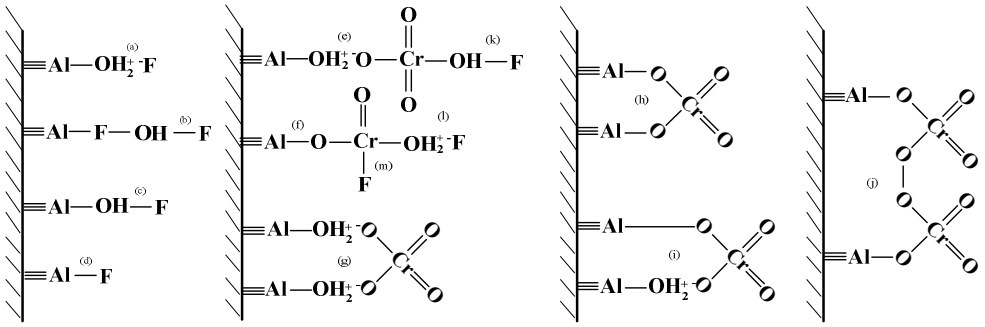

Fig.7 Diagram of proposed adsorption mechanism of fluoride and Cr(VI) species onto MA adsorbent (≡AlOH represents a surface hydroxyl site)

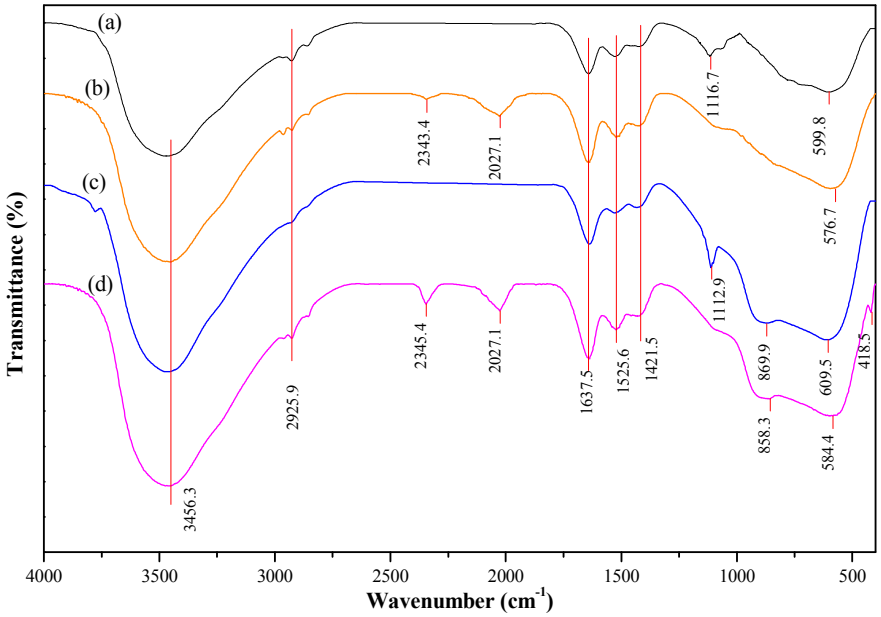

Fig.8 FT-IR spectra of (a) pristine MA adsorbent, (b) F-loaded adsorbent , (c) Cr(VI)-loaded adsorbent and (d) F and Cr(VI) co-loaded adsorbent

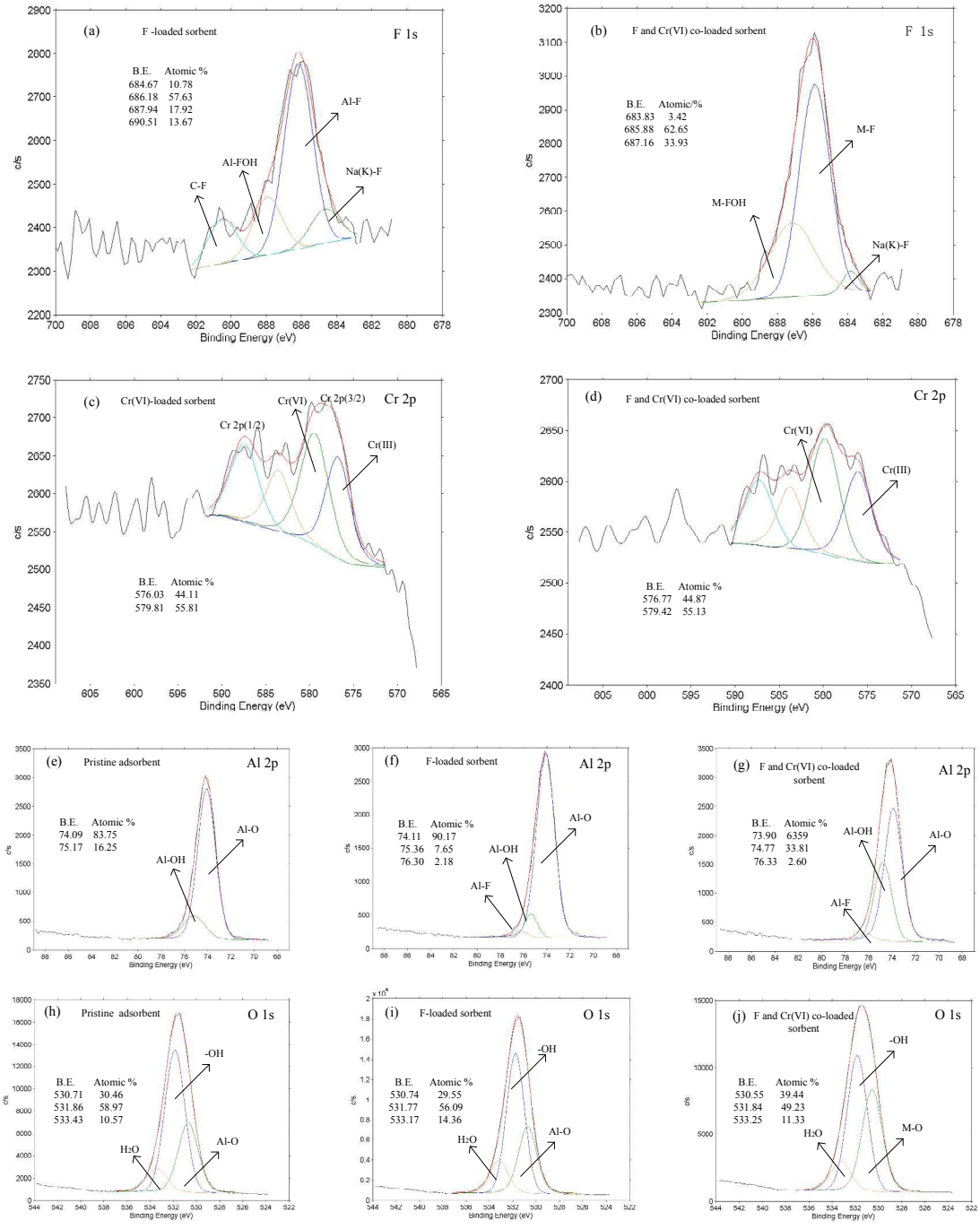

Fig.9 XPS spectra of (a) F 1s, Cr 2p, Al 2p and O 1s for MA adsorbent before and after single or simultaneous adsorded F^- and Cr(VI)

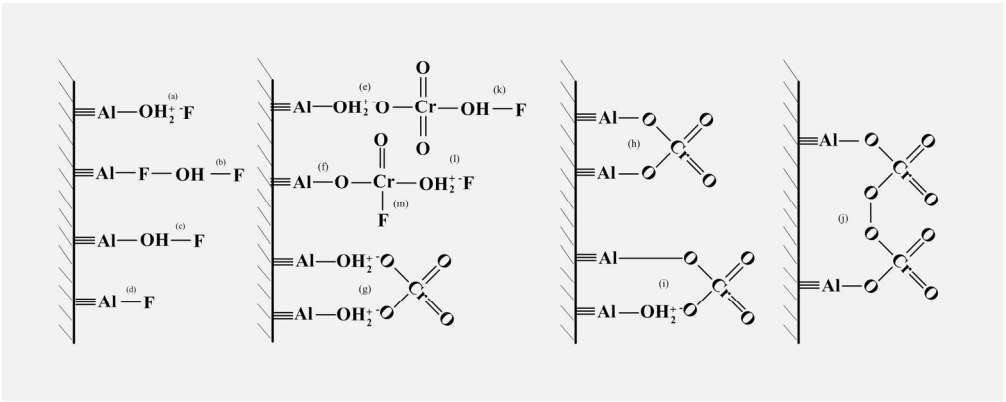

334x133mm (150 x 150 DPI)